

# Simultaneous X-ray and Optical Observations of EX Hydrae <sup>1</sup>

K. E. Belle<sup>2</sup>, S. B. Howell<sup>3</sup>, K. Mukai<sup>4,5</sup>, P. Szkody<sup>6</sup>, K. Nishikida<sup>7</sup>, D. R. Ciardi<sup>8</sup>, R. E. Fried<sup>9</sup>, J. P. Oliver<sup>10</sup>

## ABSTRACT

The intermediate polar, EX Hydrae, was the object of a large simultaneous multiwavelength observational campaign during 2000 May – June. Here we present the Rossi X-ray Timing Explorer photometry and optical photometry and spectroscopy from ground-based observatories obtained as part of this campaign. Balmer line radial velocities and Doppler maps provide evidence for an extended bulge along the outer edge of the accretion disk and some form of extended/overflowing material originating from the hot spot. In addition, the optical binary eclipse possesses an extended egress shoulder, an indication that an additional source (other than the white dwarf) is coming out of eclipse. We also compare the X-ray and optical results with the results obtained from the EUV and UV observations from the multiwavelength data set.

*Subject headings:* accretion — cataclysmic variables — stars: individual (EX Hydrae) — X-rays: stars — optical: stars

---

<sup>2</sup>X-2 MS B227, Los Alamos National Laboratory, Los Alamos, NM 87545; belle@lanl.gov

<sup>3</sup>WIYN Observatory & NOAO, P.O. Box 26732, 950 N. Cherry Ave., Tucson, AZ 85726-6732; howell@noao.edu

<sup>4</sup>NASA GSFC, Code 662 Lab. for High Energy Astrophysics, Greenbelt, MD 20771; mukai@milkyway.gsfc.nasa.gov

<sup>5</sup>Also Universities Space Research Association

<sup>6</sup>University of Washington, Dept. of Astronomy, Box 351580 Seattle, WA 98195; szkody@astro.washington.edu

<sup>7</sup>University of California, Berkeley, Space Sciences Lab, Berkeley, CA 94720; kaori@ssl.berkeley.edu

<sup>8</sup>Michelson Science Center/Caltech, 770 S. Wilson Ave., Mail Code: 100-22, Pasadena, CA 91125; ciardi@ipac.caltech.edu

<sup>9</sup>Braeside Obs., P.O. Box 906 Flagstaff, AZ 86002-0906

<sup>10</sup>University of Florida, Dept. of Astronomy, PO Box 112055 Gainesville, FL 32611; oliver@astro.ufl.edu

## 1. INTRODUCTION

Intermediate polars (IPs) are a class of magnetic cataclysmic variable (CV) in which an asynchronously rotating white dwarf accretes matter from an accretion disk via magnetically controlled accretion curtains. Modulations observed over the white dwarf spin period in IPs are generally attributed to either photoelectric absorption by the accretion curtain (the accretion curtain model, Cordova et al. 1985; Rosen et al. 1988) or to a self-eclipse of the lower accretion pole by the white dwarf (e.g., Beuermann & Osborne 1988). Over the binary orbital period, the observed modulation is due to the properties of a typical CV (accretion disk, eclipses by the secondary) and also eclipses of the emitting regions close to the white dwarf surface.

Here we report on simultaneous X-ray and optical photometric and optical spectroscopic observations of the IP EX Hydrae. EX Hya has a spin period of 67 minutes (the spin phase is denoted as  $\phi_{67}$  throughout) and a binary orbital period of 98 minutes (binary phase is denoted as  $\phi_{98}$  throughout). The mass of the white dwarf has yet to be constrained completely, as optical and UV studies give  $M_{\text{WD}} \sim 0.8 M_{\odot}$  (e.g., Hellier et al. 1987; Belle et al. 2003), while X-ray studies give  $M_{\text{WD}} \sim 0.5 M_{\odot}$  (e.g., Fujimoto & Ishida 1997; Hoogerwerf et al. 2004). Reports on recent X-ray spectroscopic observations of EX Hya can be found in Mauche et al. (2001), Mauche et al. (2003), Mukai et al. (2003), and Hoogerwerf et al. (2004). Mauche et al. (2001) and Mauche et al. (2003) find that the hot,  $T_e \sim 12$  MK, emitting plasma in the accretion column has an electron density of  $n_e = 1.0^{+2.0}_{-0.5} \times 10^{14} \text{ cm}^{-3}$ , using Chandra High Energy Transmission Grating (HETG) spectra. Mukai et al. (2003) find that the Chandra HETG spectrum of EX Hya can be fit with a simple isobaric cooling flow model. Hoogerwerf et al. (2004) use the Chandra spectrum to find a radial velocity and mass for the white dwarf,  $K_1 = 58.2 \pm 3.7 \text{ km s}^{-1}$  and  $M_{\text{WD}} = 0.49 \pm 0.13 M_{\odot}$ .

This paper is the third and final paper in a series detailing simultaneous multiwavelength observations of EX Hya. In the first paper (Belle et al. 2002), we reported on observations with the *Extreme Ultraviolet Explorer* (*EUVE*); its one million seconds of photometry and spectroscopy of EX Hya provided the basis for the multiwavelength observations. The EUV photometry revealed the presence of two dips in the binary light curve, whose absorption depths changed with spin phase. Our second paper (Belle et al. 2003) presented *Hubble Space Telescope* (*HST*) spectroscopy of EX Hya. The mass of the white dwarf was calculated as  $M_{\text{WD}} = 0.91 \pm 0.05 M_{\odot}$  from the  $K$  amplitude of the radial velocity curve of the narrow UV emission lines. Spectral model fits to the UV data also produced the same mass white

---

<sup>1</sup>Based in part on observations obtained with the Apache Point Observatory 3.5-meter telescope, which is owned and operated by the Astrophysical Research Consortium.

dwarf with  $T = 23,000$  K and an accretion disk truncated at  $2.5 R_{\text{WD}}$ .

## 2. OBSERVATIONS

As part of a simultaneous multiwavelength observational campaign of EX Hya (executed in 2000 May – June, see Belle et al. 2002, 2003), we obtained X-ray photometry from the Rossi X-ray Timing Explorer satellite (*RXTE*), optical spectroscopy from Apache Point Observatory (APO) and optical photometry from Braeside Observatory (BO) and Rosemary Hill Observatory (RHO). Table 1 gives a complete list of the simultaneous EX Hya observations completed during 2000 May – June; those marked with an asterisk are presented in this paper.

*RXTE* observed EX Hya for 15 ks over four separate observations using the Proportional Counter Array, which consists of five Proportional Counter Units (PCUs). During the observations, only PCU2 and PCU3 were in continuous operation, so we present here only the data from these two PCUs. The data set spans the wavelength range  $1 - 5$  Å ( $12.4 - 2.5$  keV) and provides complete coverage of the spin period but only partial coverage of the binary period, lacking binary phases  $\phi_{98} = 0.30 - 0.39$ . Sixteen nights of *BVR* photometry were obtained from BO and 10 nights of *I* photometry were obtained from RHO. Complete binary and spin phase coverage was obtained with all of the optical photometry.

Blue and red spectra were obtained during two nights of observations, 2000 May 15 and 28 (UT), with the 3.5 m telescope at APO, which provided complete coverage of the binary and spin phases of EX Hya. The observations utilized the Double Imaging Spectrograph and obtained high resolution ( $0.80$  Å pixel $^{-1}$ ) blue spectra in the wavelength range  $4185 - 5010$  Å and high resolution ( $1.17$  Å pixel $^{-1}$ ) red spectra in the wavelength range  $6285 - 7320$  Å. These wavelength ranges include the H $\gamma$   $\lambda 4340.5$ Å, H $\beta$   $\lambda 4861.3$ Å, and H $\alpha$   $\lambda 6562.8$ Å emission lines.

## 3. ANALYSIS

### 3.1. X-ray and Optical Photometry

#### 3.1.1. Period Analysis

We first searched for periods in each of our photometric data sets using the phase dispersion minimization (PDM) routine (Stellingwerf 1978), a technique for finding periods

in a data set by minimizing scatter about a light curve. For a given input data set and range of test frequencies, PDM will compute a light curve and a binned light curve from the input data for each test frequency, and the dispersion of the data about the mean light curve. The dispersion of the data will be at a minimum when a 'real' frequency is found. This is reflected in the value of  $\Theta$  that PDM calculates. A two-sided F-test can then be used to calculate the confidence of a given frequency for which  $\Theta$  is at a minimum.

The PDM results are shown as thetagrams in Figure 1 for the  $B$ ,  $I$ , and  $RXTE$  photometry. Thetagrams were also created for the  $V$  and  $R$  photometric data, but are similar to the  $B$  thetagram (the same frequencies are found), so are not presented here. Strong frequencies in the  $B$  and  $I$  thetagrams, above the 95% confidence level, include the spin frequency,  $\omega$ , the binary frequency,  $\Omega$ , harmonics of these two frequencies,  $\omega/2$  and  $2\Omega$ , and the beat frequencies,  $\omega - \Omega$  and  $\omega - 2\Omega$ . They have been labeled on the  $RXTE$  and  $B$  plots in Figure 1 and are listed in Table 2. The 99% confidence levels have been denoted on the plots as dotted lines. The frequencies shortward of  $\sim 6 \text{ day}^{-1}$  represent the length of the observations and also the time between data sets.

The strongest frequency in each thetagram is  $\omega$ , with  $\Theta = 0.76$  ( $RXTE$ ), 0.42 ( $B$ ), and 0.56 ( $I$ ). Though several other frequencies appear above the 95% confidence level in the  $RXTE$  thetagram, the time-limited nature of the photometric data precludes us from drawing many conclusions about the observed frequencies. The most we can say is that the possible appearance of the beat frequencies  $\omega - \Omega$  and  $\omega - 2\Omega$  may be interesting, but more data is required to confirm their existence. We would also like to note that during the  $RXTE$  observation, the satellite orbital period was 95.73 min, which is very close to the 98.26 min orbital period of EX Hya. The satellite orbital period would contribute to a peak in frequency near the binary orbital period in the  $RXTE$  thetagram.  $\Theta$  values for statistically significant frequencies are given in Table 3.

Previous period analyses of X-ray photometry of EX Hya are limited. A search of the literature found only one instance: Allan et al. (1998) produced a power spectrum of their 40 ks ASCA observation (0.6 – 10.0 keV), which shows peaks at  $\omega$  and  $\Omega$ . Optical thetagrams are a bit more common and a nice example can be found in Siegel et al. (1989), who report the appearance of the frequencies  $\omega$ ,  $\Omega$ ,  $\Omega/2$ , and  $\omega \pm 2\Omega$ . The appearance of  $\omega - \Omega$  is questionable in the Siegel et al. (1989) data set, and  $\omega + \Omega$  is not seen. While  $\omega + \Omega$  is also not seen in our data sets,  $\omega - \Omega$  is prominent. Emission at the beat frequency  $\omega - \Omega$  is due to reprocessed light from the secondary and hot spot along with orbital absorption of emission from the white dwarf and reprocessed light from the inner accretion disk and accretion stream. The appearance of this frequency in our data set suggests that something has changed within the binary system that would contribute to emission and absorption at

the  $\omega - \Omega$  beat frequency, which is most likely an extended hot spot region along the outer edge of the disk. We will explore the appearance of the  $\omega - \Omega$  beat frequency further in §3.2.1.

### 3.1.2. *RXTE Photometry*

Photometric data obtained from *RXTE* are shown in Figure 2 phased on the binary ephemeris,  $T = 2437699.94179 + 0.068233846(4)\text{E}$ , and spin ephemeris,  $T = 2437699.8914(5) + 0.046546504(9)\text{E} - 7.9(4) \times 10^{-13}\text{E}^2$ , (binned to 0.02 in phase) of Hellier & Sproats (1992). The binary phased light curve, shown in the left panel of Figure 2, exhibits an eclipse at  $\phi_{98} \sim 0.0$  of the X-ray emitting region near the white dwarf surface.<sup>2</sup> In addition to the binary eclipse, the light curve also displays quite a bit of variability throughout its entirety. This is a result of the combined effects of the X-ray flickering behavior of EX Hya and the poor phase coverage of the *RXTE* data. Each phase bin was covered only once or twice during the entire observation, in which case any flickering in individual cycles of EX Hya will not be averaged out. In particular, the flickering seen at  $\phi_{98} \sim 0.65$  should not be confused with the bulge eclipse at  $\phi_{98} \sim 0.7$  seen in lower energy X-ray data ( $< 2$  keV, e.g., Cordova et al. 1985; Rosen et al. 1988).

The binary phased light curve has had the sinusoidal spin modulation subtracted. On an absolute count rate scale, it can be seen that the binary eclipse does not go to zero, implying a partial eclipse of the X-ray emitting regions. This is a result of the lower accreting pole being eclipsed by the secondary, while the upper pole remains in view. Unfortunately, our *RXTE* data set is not extensive enough to analyze binary light curves extracted at different phase segments of the spin period.

In creating the spin phased light curve, shown in the right panel of Figure 2, we omitted data from binary phases  $\phi_{98} = 0.95 - 1.01$ , which correspond to the binary eclipse. The X-ray flickering present in the binary phased light curve is also seen throughout the spin phased light curve. Ignoring this flickering, one can see that the data folded over spin phase exhibit a roughly sinusoidal modulation, peaking at  $\phi_{67} \sim 0$ , which is the signature of a rotating white dwarf accreting at both magnetic poles. The sinusoidal fit to the spin phased data was created omitting the dip at  $\phi_{67} \sim 0.8$ ; the solution of the form  $A + B \sin(\phi_{67} - \phi_0)$  is given in Table 4.

---

<sup>2</sup>The sinusoidal form of the  $O - C$  values given in Hellier & Sproats (1992) gives  $O - C = -0.005 P_{\text{orb}}$  for the 2000 May – June observations. Given the moderate time resolution of our data as presented, this shift in phase will be unnoticeable.

### 3.1.3. Optical Photometry

Figure 3 displays the optical photometry of EX Hya folded on the spin ephemeris and binned to 0.02 in phase. Marked on the Figure are the spin phase designations of maximum ( $\phi_{67} = 0.99 - 1.24$ ), minimum ( $\phi_{67} = 0.49 - 0.74$ ), rise ( $\phi_{67} = 0.74 - 0.99$ ), and decline ( $\phi_{67} = 0.24 - 0.49$ ), which will be used for the analysis of the photometry folded on the binary orbital period. Data from the binary eclipse,  $\phi_{98} = 0.95 - 1.01$ , have been omitted in the spin phased light curves. The *BVR* light curves are modulated sinusoidally (solutions for the sinusoidal fits of the form  $A + B \sin 2\pi(\phi_{67} - \phi_0)$  are given in Table 4) and peak at  $\phi_{67} = 0.12 \pm 0.02$ . The *I* light curve contains quite a bit of “wobble”, which is a result of modulations over the binary orbital period translating into the spin phasing. We do not believe that any of the *I* modulation is due to the secondary star. The optical spectra (out to 7200Å) as well as an infrared spectrum obtained by one of us (SBH) during the campaign do not reveal any spectral features that could be associated with the secondary.

The maximum phase of  $\phi_{67} = 0.12$  of the spin phased light curves matches well with the value of  $\phi_{67} = 0.115 \pm 0.001$  determined from our *EUVE* photometry (Belle et al. 2002), but differs from the value of  $\phi_{67} \approx 0.0$  obtained using the UV continuum flux from our *HST* data (Belle et al. 2003), and also the value of  $\phi_{67} \sim 0$  we determine in this paper for the X-ray photometry. The discrepancy between the phases of spin maximum will be addressed in §4.

Figure 4 displays representative light curves of the optical photometry folded on the binary ephemeris. The left panel of Figure 4 shows the *B* binary phased light curve after the sinusoidal spin modulation has been subtracted. The right panel of Figure 4 shows the *B* data separated into spin maximum (top) and spin minimum (bottom). Each light curve has been binned to 0.02 in phase. The light curves exhibit typical behavior of an eclipsing binary system, with an eclipse near phase  $\phi_{98} = 0.0$ . This eclipse has typically been associated with an occultation of (part of) the white dwarf by the secondary star. Recently, though, it was questioned if this was a white dwarf eclipse, as the binary eclipse in EUV data of EX Hya appears at  $\phi_{98} = 0.97$  (Belle et al. 2002); it was suggested that the optical eclipse was that of the hot spot on the outer edge of the accretion disk. Eclipse timings by Siegel et al. (1989) show that the eclipse minimum shifts between spin phases  $\phi_{67} \sim 0.25$  and  $\phi_{67} \sim 0.75$  by about 20 s. Assuming a binary separation of  $a \simeq 5 \times 10^{10}$  cm, they determine that the shift in eclipse minimum corresponds to an eclipse of material located (roughly) on the white dwarf surface. While our data do not have the high time resolution required to perform a detailed analysis such as this, close inspection of the unbinned light curves shows that the binary eclipse during  $\phi_{67} \sim 0.75$  (rise) occurs ahead of the binary eclipse during  $\phi_{67} \sim 0.25$  (decline) by  $\sim 20$  s, consistent with the earlier results of Siegel et al. (1989).

The spin separated light curves shown in the right panel of Figure 4 reveal additional

information about the binary system. Inspection of the binary eclipse shows an extended egress shoulder on the spin minimum eclipse. This behavior is also seen in  $V$ ,  $R$ , and  $I$ . This shoulder would be caused by an extended object (as compared with the white dwarf) coming out of eclipse, such as the bulge along the outer edge of the accretion disk, or, as we will discuss later, a region at the inner accretion disk radius where an overflow stream impacts with the magnetosphere (such a geometry would be favored during spin minimum). A similar feature in the binary eclipse has also been reported by Hellier et al. (2000) for EX Hya during outburst.

### 3.2. Optical Spectroscopy

APO spectra from 2000 May 28 are shown in Figures 5 and 6. Figure 5 presents the mean blue and red spectra, which contain strong Balmer emission lines, as well as He I and He II emission. Figure 6 presents velocity line profiles of the  $H\gamma$ ,  $H\beta$ , and  $H\alpha$  emission lines plotted over the binary orbital period. The lines exhibit a double-peaked shape over all binary phases, indicative of emission from an accretion disk, and have average FWHM values of  $\sim 50\text{\AA}$ , or  $\sim 2000 - 3000\text{ km s}^{-1}$ .

#### 3.2.1. The S-wave Component

The S-wave component of the emission lines, contributed by the hot spot on the outer edge of the accretion disk, is clearly visible as a red-shifted or blue-shifted component in the  $H\alpha$ ,  $H\beta$ , and  $H\gamma$  emission lines throughout most binary phases. The exact behavior of the S-wave component varies between the emission lines. In  $H\alpha$ , the S-wave is red-shifted during the early binary phases of  $\phi_{98} = 0.03 - 0.38$  and has strongest zero-velocity emission during  $\phi_{98} = 0.4 - 0.5$ , the phases during which we are afforded a view of the hot spot on the opposite side of the accretion disk. The S-wave component is blue-shifted from  $\phi_{98} = 0.51 - 0.60$ , is missing (or at least much less prominent) from  $\phi_{98} = 0.64 - 0.85$ , the phases during which we would expect to see the hot spot directly on the near edge of the disk, and is red-shifted again at  $\phi_{98} = 0.90 - 0.99$ .

In the  $H\beta$  and  $H\gamma$  emission lines, the S-wave component follows the general behavior of that seen in the  $H\alpha$  line, with a few exceptions. The S-wave component is at zero velocity at  $\phi_{98} \sim 0$  and  $\phi_{98} \sim 0.3$ , where the  $H\alpha$  S-wave component is red-shifted. It also becomes blue-shifted at earlier phases, around  $\phi_{98} \sim 0.4$  for both the  $H\beta$  and  $H\gamma$  lines, while it is still at zero-velocity in the  $H\alpha$  line. The S-wave component also appears to bounce back and

forth between being red- and blue-shifted during binary phases  $\phi_{98} = 0.60 - 0.85$ . Another intriguing feature of the  $H\gamma$  and  $H\beta$  emission lines during these phases is that there is little to no zero-velocity emission.

Taking the general behavior of the S-wave component from all three lines, we can infer geometric properties of the hot spot and bulge on the outer edge of the accretion disk. The S-wave component is red-shifted from  $\phi_{98} \sim 0.85 - 0.3$ , at zero velocity around  $\phi_{98} \sim 0.3 - 0.4$ , and is blue-shifted from  $\phi_{98} \sim 0.4 - 0.6$ . After  $\phi_{98} \sim 0.6$ , the S-wave component disappears. The zero velocity emission phase at  $\phi_{98} \sim 0.3 - 0.4$  tells us that the S-wave component is dominated by emission on the opposite side of the disk, between phases  $\phi_{98} \sim 0.8 - 0.9$  on the accretion disk. This emission therefore appears as a red-shifted component from  $\phi_{98} \sim 0.85 - 0.3$ . The S-wave is only blue-shifted when this component moves toward the observer, during phases  $\phi_{98} = 0.4 - 0.6$ . At phase  $\phi_{98} = 0.6$ , material begins to obscure our view of the hotter parts of the hot spot, and so the S-wave component disappears. From the missing S-wave emission during phases  $\phi_{98} = 0.60 - 0.85$ , and the absence of any zero velocity component in the emission lines, we can infer that there is vertically extended material along the outer edge of the disk obscuring the S-wave and zero velocity components starting at  $\phi_{98} \sim 0.6$ . This extended material is likely irradiated along its inner edge by the white dwarf, and gives rise to the S-wave emission.

Further evidence for extended emission along the outer edge of the disk is seen in the Doppler tomogram for the  $H\alpha$  emission line, displayed in Figure 7. The tomograms shown in the Figure are measured from spectra obtained on 2000 May 28 and are plotted over binary orbital phase. The  $H\alpha$  tomogram shows enhanced emission along the outer edge of the accretion disk, for approximately 0.5 in phase. Extended emission along the outer edge of the accretion disk is also indirectly observed in the EUV data of EX Hya, in the form of absorption of the EUV emitting region (Belle et al. 2002). This absorption also lasts for approximately half of an orbital phase.

Each tomogram exhibits a bright area of emission at  $\phi_{98} \sim 0.8$  – this is the hot spot and is the origin of the S-wave component. The  $H\gamma$  and  $H\beta$  tomograms also show enhanced emission that appears to extend from the region at  $\phi_{98} \sim 0.8$  toward the inner regions of the disk ( $R_{\text{in}} \lesssim 6.5 R_{\text{WD}}$ , see §3.2.2). Hellier et al. (2000) observed evidence of disk overflow in EX Hya during its 1998 outburst. In X-rays, the overflow stream was indirectly observed as an  $\omega - \Omega$  beat modulation, and in the optical, the overflow stream was detected via its eclipse and from line emission at the site of the stream impact with the magnetosphere. We checked AAVSO data of EX Hya for the time period immediately preceding and following our observations, but the available data show no evidence of an outburst. In fact, the data points for EX Hya show it sitting at 13 – 12.5 mag, which is its normal quiescent brightness.

This would rule out a period of enhanced mass transfer as the cause of the overflowing material inferred from our data, as such an event would likely be indicated by an increase of the system brightness.

Tomograms plotted over the white dwarf spin phase were also constructed; however, these show no coherent emission sites. It has also been shown previously (Hellier 1999) that tomograms of EX Hya folded on the spin phase reveal little information.

### 3.2.2. Radial Velocities

Measuring the central wavelengths of the H emission lines proved to be a challenge, as the double-peaked nature of the lines and the contribution of the S-wave component made it difficult to use a single Gaussian profile for determining line parameters. We therefore used a method for fitting a double-Gaussian profile to the emission lines, which measures radial velocities from emission line wings (D. W. Hoard 2004, private communication, for a description of double-Gaussian fitting see Shafter 1983; Shafter et al. 1986).

We created radial velocity curves for the  $H\gamma$ ,  $H\beta$ , and  $H\alpha$  emission lines. Figure 8 displays the radial velocity curves for the  $H\alpha$  and  $H\beta$  lines. Strong asymmetries due to emission from the hot spot prevented accurate determinations of  $K_1$  or  $\gamma$  from fitted sine curves, but a fit of the form  $v = \gamma + K_1 \sin 2\pi(\phi_{98} - \phi_0)$  to the  $H\alpha$  line (shown on Figure 8) gives  $\gamma = -14 \pm 1 \text{ km s}^{-1}$ ,  $K_1 = 61 \pm 6 \text{ km s}^{-1}$ , and  $\phi_0 = 0.115 \pm 0.016$ . The  $K_1$  value of  $61 \pm 6 \text{ km s}^{-1}$  is in agreement with our previous value of  $K_1 = 59.6 \pm 2.9 \text{ km s}^{-1}$  determined from narrow UV emission lines (Belle et al. 2003), but slightly lower than a previous value of  $69 \pm 9 \text{ km s}^{-1}$  determined from optical emission lines by Hellier et al. (1987).

We also calculated the radial velocity of the S-wave component in each of the H emission lines. We found that the velocity amplitude of the S-wave emission places the emission site at  $9 \times 10^{10} \text{ cm}$  from the center of the white dwarf for the  $H\alpha$  component and at  $3 \times 10^{10} \text{ cm}$  from the center of the white dwarf for the  $H\beta$  and  $H\gamma$  components. The smaller value obtained from the  $H\beta$  and  $H\gamma$  radial velocities may be due to contamination from the overflowing material. If we assume that the S-wave component originates at the outer edge of the accretion disk, the placement of the  $H\alpha$  S-wave component gives an outer disk radius of  $R_{\text{out}} \sim 10^{11} \text{ cm}$ . The inner accretion disk radius may be measured from the high velocity emission line wings, which extend at least to  $1500 \text{ km s}^{-1}$  (Figure 6). This velocity gives an upper limit to the inner disk radius of  $R_{\text{in}} = 6.5 R_{\text{WD}} = 5 \times 10^9 \text{ cm}$  for a  $0.8 M_{\odot}$  white dwarf or  $R_{\text{in}} = 2.9 R_{\text{WD}} = 3 \times 10^9 \text{ cm}$  for a  $0.5 M_{\odot}$  white dwarf.

#### 4. COMPARISON OF DATA AT ALL WAVELENGTHS

A comparison of data from all wavelength regimes can lead us to an overall picture of EX Hya. Signatures of an extended bulge along the outer edge of the accretion disk are seen in the EUV photometry as absorption of the EUV emitting region on the white dwarf surface, in the optical spectroscopy as enhanced emission in the  $H\alpha$  emission line tomogram, and as absorption of the zero velocity components of the  $H\beta$  and  $H\gamma$  emission lines during certain binary phases. The absorption at phases  $\phi_{98} = 0.55 - 1.1$  in the EUV photometry match well with the absorption in the  $H\beta$  and  $H\gamma$  emission lines, seen at  $\phi_{98} = 0.6 - 0.9$ . The fact that the bulge is not present as a source of continuum emission in the binary phased light curves implies that the bulge material is optically thin.

Some form of overflowing material is seen in the Doppler tomograms of the  $H\gamma$  and  $H\beta$  emission lines as enhanced emission extending from the hot spot toward the inner edge of the accretion disk. Other evidence for overflowing material comes from the blue-shifted velocities of the Balmer lines at  $\phi_{98} \sim 0.4$ . One may also infer the existence of an extended/overflowing hot spot from the extended egress shoulder of the binary eclipse during spin minimum phases, which implies that an additional source, other than the white dwarf, is coming out of eclipse.

Some inconsistencies remain. The first is the phase of spin maximum as derived from light curves of continuum and emission line fluxes. X-ray spin maximum occurs at  $\phi_{67} \sim 0$ , EUV at  $\phi_{67} = 0.115 \pm 0.001$ , UV continuum at  $\phi_{67} = 0.01 \pm 0.05$ , UV emission lines at  $\phi_{67} = (0.05 - 0.08) \pm 0.05$ , and optical at  $\phi_{67} = 0.12 \pm 0.02$ . The difference in the phase of spin maximum has been reported previously by Hellier et al. (2000) for their simultaneous X-ray and optical observations. An extended accretion region on the white dwarf surface would be an initial suggestion for the difference in phase of spin maximum; however, one would expect that the high energy spin maxima would be coincident, but this is not the case.

Another inconsistency is the phase of the binary eclipse across wavelength regimes. X-ray and optical data show the binary eclipse at  $\phi_{98} \approx 0.0$ , while EUV data displays two eclipses near, but not at,  $\phi_{98} = 0$ : one at  $\phi_{98} = 0.97$  and the other at  $\phi_{98} = 1.04$ . The EUV eclipse at  $\phi_{98} = 1.04$  could be an eclipse of the disk overflow stream impact with the magnetosphere, though this region would not be expected to be bright in the EUV. But there still remains the phase difference of the binary eclipse. The difference between the EUV and X-ray eclipses could be reconciled by the fact that the *RXTE* coverage of those phase bins is not nearly as extensive as the *EUVE* coverage. Perhaps observations that provide better phase sampling would show the X-ray eclipse slightly earlier in phase. In such a case, then, a physical displacement between the higher and lower energy emitting regions could be the cause of the phase difference of the binary eclipses.

## 5. CONCLUSIONS

We have presented simultaneous X-ray and optical photometry and optical spectroscopy of the IP EX Hya obtained as part of a large multiwavelength observational campaign of EX Hya. The data provide evidence for an extended bulge along the outer edge of the accretion disk, corroborating our EUV results (Belle et al. 2002). Over the binary orbital period, the zero-velocity component of the optical emission lines is seen to be absorbed during binary phases  $\phi_{98} = 0.6 - 0.85$ . The  $H\alpha$  tomogram also shows enhanced emission along the outer edge of the accretion disk at phases  $\phi_{98} = 0.6 - 0.85$ . The  $H\beta$  and  $H\gamma$  tomograms also indicate that some amount of material may be extended from the hot spot toward the inner regions of the accretion disk.

Combined together, the data suggest that EX Hya may be experiencing a period of enhanced mass transfer, as the data presented here bear similarities to the outburst data of 1998. The system remained, however, at its quiescent brightness of  $\sim 13$  mag during the observations. Perhaps there was a period of enhanced mass transfer that was not recorded, or EX Hya may not have returned entirely to its quiescent state after outburst. Finally, we would like to call the attention of the reader to an initial light curve of EX Hya published by Mumford (1967, Fig. 5) prior to knowledge of EX Hya as an IP (i.e., no spin modulation was subtracted from the light curve). This light curve (which has  $\Delta m \sim 0.4$  between eclipses) shows none of the modulation associated with the white dwarf spin period that is so prevalent in our 2000 photometric data ( $\Delta m \sim 0.7$  between eclipses). Obviously, conditions within EX Hya, e.g., a larger bulge or extended accretion curtains, have changed in order to produce the enhanced emission. It is apparent that obtaining over one million seconds of data has only increased the number of questions we have about EX Hya.

KEB thanks P. Bradley for very helpful discussions and D. W. Hoard for providing his double-Gaussian fitting routines. We thank Dr. Jean Swank, the RXTE project scientist, for the allocation of the Target of Opportunity observing time, and the RXTE Science Operations Center for scheduling these observations.

## REFERENCES

- Allan, A., Hellier, C., & Beardmore, A. 1998, MNRAS, 295, 167
- Belle, K. E., Howell, S. B., Sirk, M. M., & Huber, M. E. 2002, ApJ, 577, 359
- Belle, K. E., Howell, S. B., Sion, E. M., Long, K. S., & Szkody, P. 2003, ApJ, 587, 373

- Beuermann, K. & Osborne, J. P. 1988, *A&A*, 189, 128
- Córdova, F. A., Mason, K. O., & Kahn, S. M. 1985, *MNRAS*, 212, 447
- Fujimoto, R. & Ishida, M. 1997, *ApJ*, 474, 774
- Hellier, C. 1999, *ApJ*, 519, 324
- Hellier, C., Kemp, J., Naylor, T., Bateson, F. M., Jones, A., Overbeek, D., Stubbings, R., & Mukai, K. 2000, *MNRAS*, 313, 703
- Hellier, C., Mason, K. O., Rosen, S. R., & Córdova, F. A. 1987, *MNRAS*, 228, 463
- Hellier, C. & Sproats, L. N. 1992, *IBVS*, 3724
- Hoogerwerf, R., Brickhouse, N. S., & Mauche, C. W. 2004, *ApJ*, 610, 411 (astro-ph/0403665)
- Mauche, C. W., Liedahl, D. A., & Fournier, K. B. 2001, *ApJ*, 560, 992
- Mauche, C. W., Liedahl, D. A., & Fournier, K. B. 2003, *ApJ*, 588, L101
- Mumford, G. S. 1967, *ApJS*, 15, 1
- Mukai, K., Kinkhabwala, A., Peterson, J. R., Kahn, S. M., & Paerels, F. 2003, *ApJ*, 586, L77
- Rosen, S. R., Mason, K. O., & Córdova, F. A. 1988, *MNRAS*, 231, 549
- Shafter, A. W. 1983, *ApJ*, 267, 222
- Shafter, A. W., Szkody, P., & Thorstensen, J. R. 1986, *ApJ*, 308, 765
- Siegel, N., Reinsch, K., Beuermann, K., van der Woerd, H., & Wolff, E. 1989, *A&A*, 225, 97
- Stellingwerf, R. F. 1978, *ApJ*, 224, 953

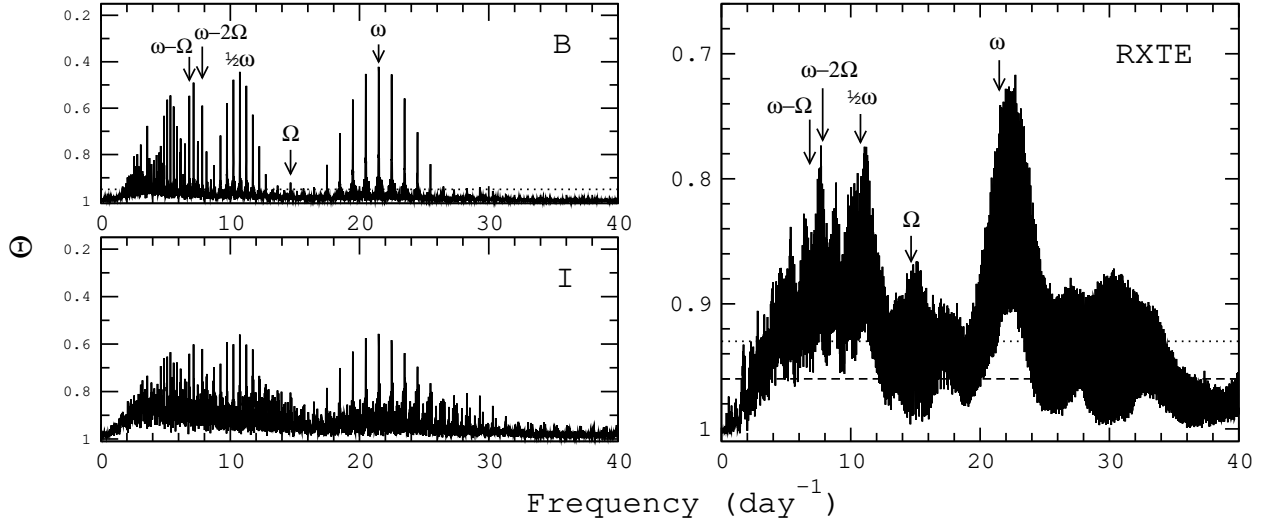


Fig. 1.— Thetagrams for the *B*, *I*, and *RXTE* photometry. A smaller  $\Theta$  value indicates a higher statistical confidence (note the y-axis has been inverted). Frequencies commonly found in IPs are labeled on the *B* and *RXTE* plots and listed in Table 2. The dotted lines represent the 99% confidence level, while the dashed line on the *RXTE* plot represents the 95% confidence level. The 99% confidence level for the *I* thetagram is at 0.99. Values of  $\Theta$  for the frequencies noted in this figure are given in Table 3.

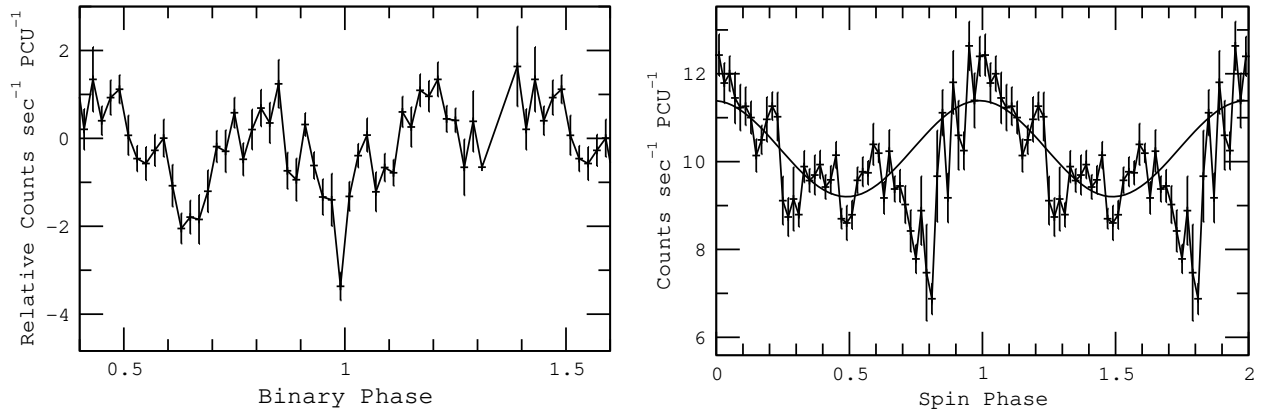


Fig. 2.— *RXTE* photometry phased on the binary and spin ephemerides. The left panel shows binary phased data after subtraction of the spin modulation. The solution for the sine curve shown fit to the spin phased data in the right panel is given in Table 4.

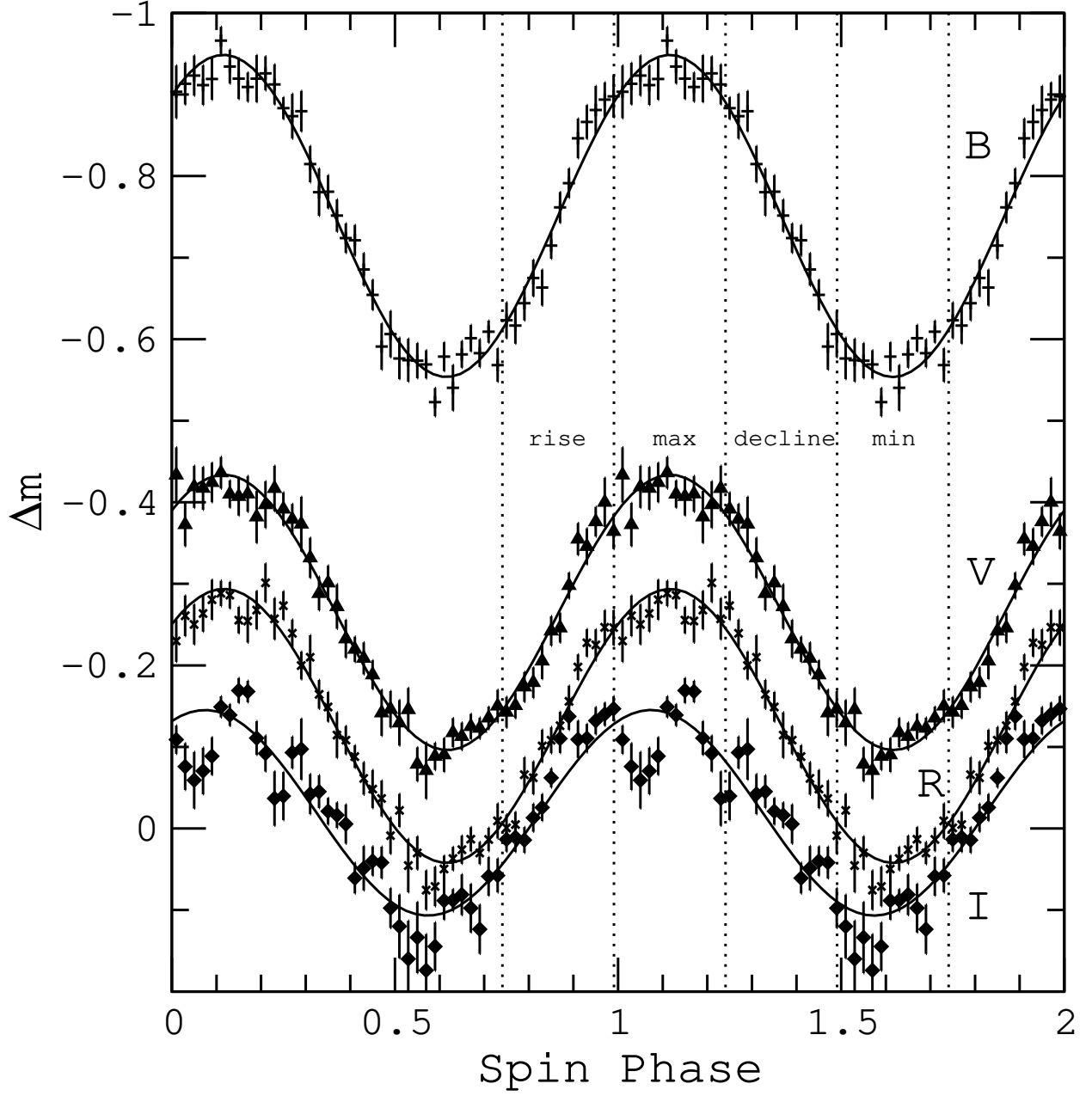


Fig. 3.— *BVRI* optical photometry folded on the spin period. A sinusoidal function is shown fit to each light curve; solutions are given in Table 4. Phase delineations are given for spin maximum ( $\phi_{67} = 0.99 - 1.24$ ), minimum ( $\phi_{67} = 0.49 - 0.74$ ), rise ( $\phi_{67} = 0.74 - 0.99$ ), and decline ( $\phi_{67} = 0.24 - 0.49$ ). The offsets between the light curves are real magnitude differences.

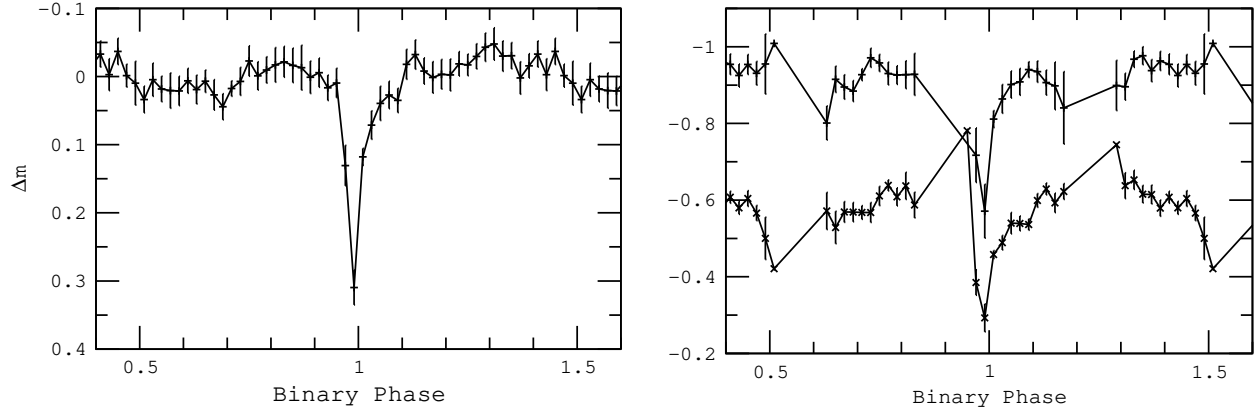


Fig. 4.—  $B$  photometric data phased on the binary period. The left panel displays the  $B$  photometry after subtraction of the sinusoidal spin modulation. The right panel displays the same photometric data separated into spin maximum (top) and spin minimum (bottom).

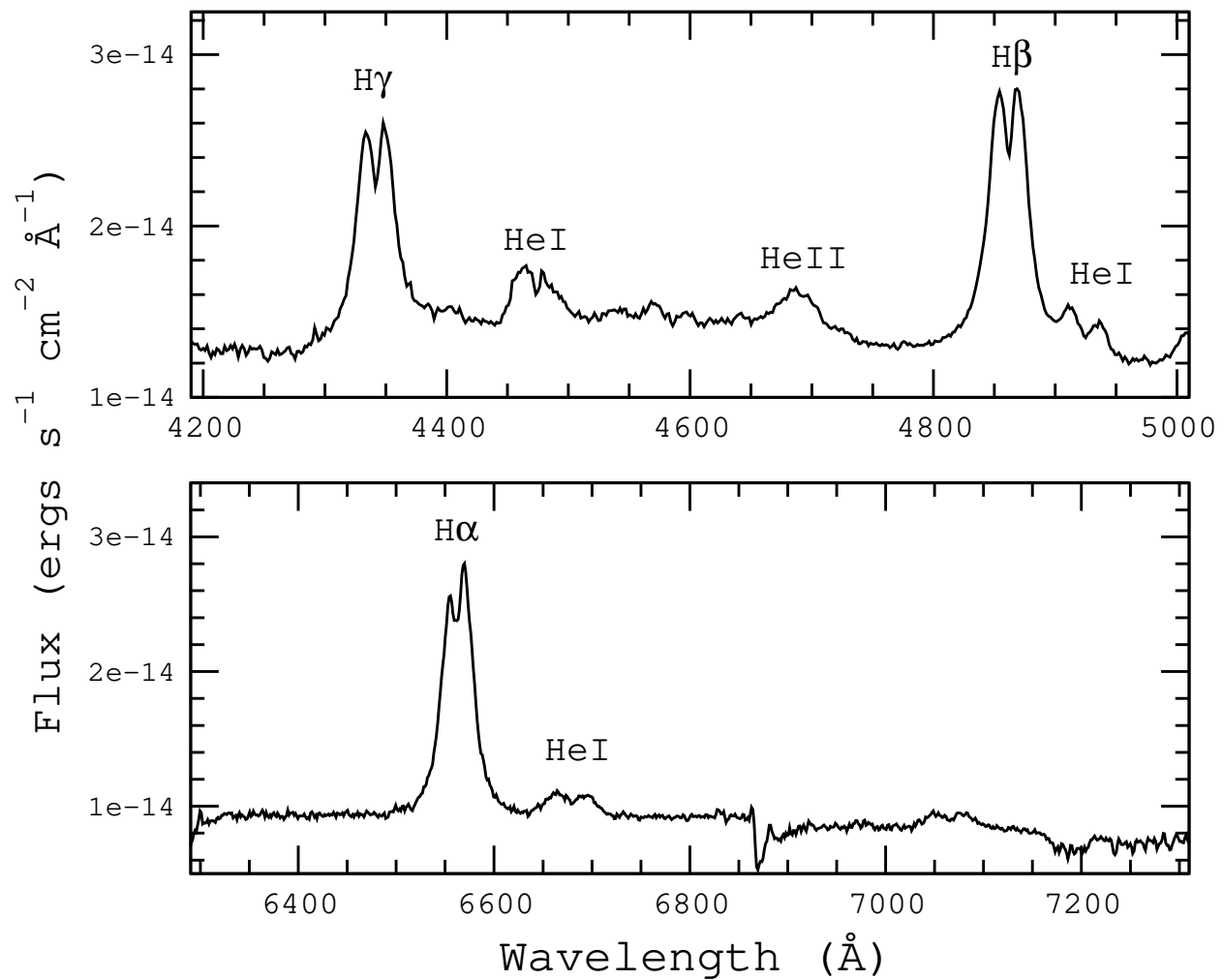


Fig. 5.— Average blue (top) and red (bottom) spectra from 2000 May 28.

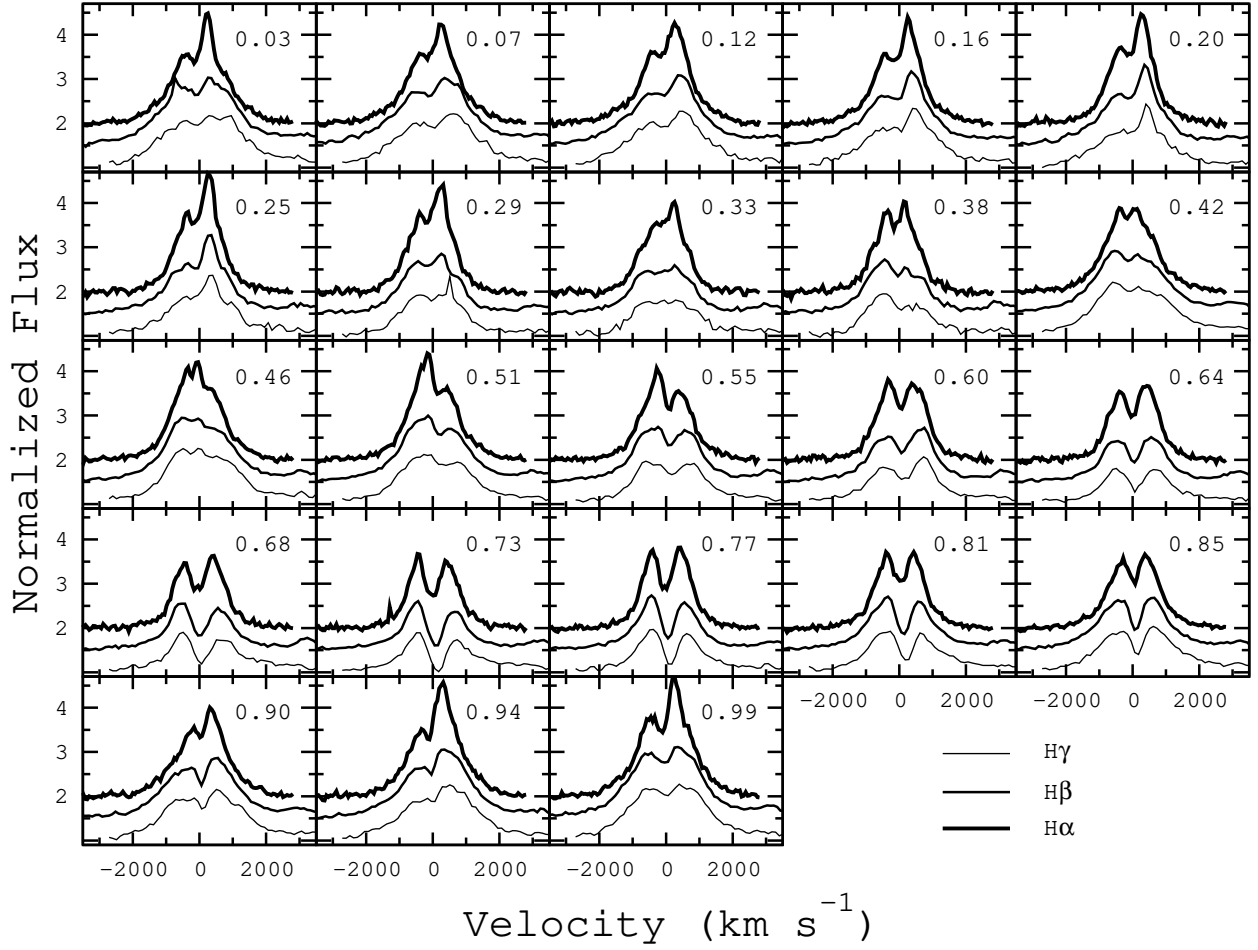


Fig. 6.— H $\alpha$ , H $\beta$ , and H $\gamma$  velocity line profiles shown over the binary orbital period (phase noted in the upper right corner of each plot) for data from 2000 May 28. The S-wave component is clearly visible as a red-shifted or blue-shifted component during most binary phases. The H $\beta$  and H $\alpha$  line profiles have been shifted upward in flux by 0.5 and 1.0, respectively.

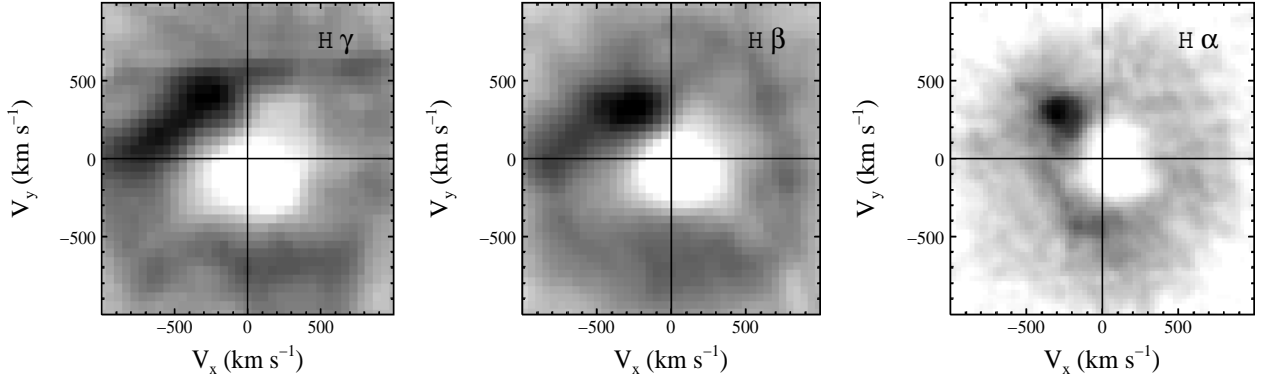


Fig. 7.— From left to right, tomograms over the binary phase for the  $H\gamma$ ,  $H\beta$ , and  $H\alpha$  emission lines from spectra obtained during the night of 2000 May 28. Each tomogram shows a bright spot at  $\phi_{98} \sim 0.8$ . The  $H\gamma$  and  $H\beta$  tomograms show enhanced emission from the hot spot toward the inner edge of the disk. Extended emission (roughly half of the orbital phase) is seen along the outer edge of the accretion disk in the  $H\alpha$  tomogram. The phasing of the tomograms follows standard convention, where binary phase 0 is at 12 o'clock on the plot and phase increases clockwise.

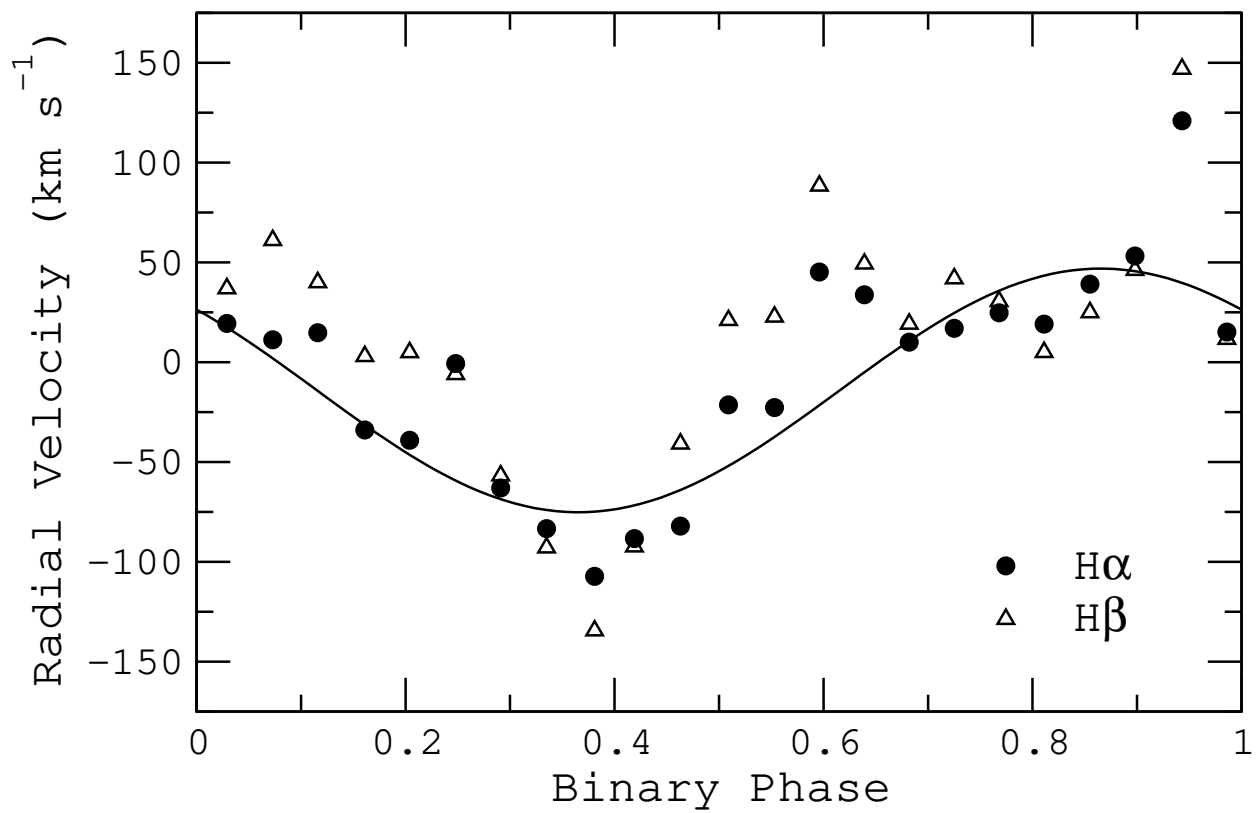


Fig. 8.— Radial velocities of the H $\alpha$  and H $\beta$  optical emission lines folded on the binary phase. The large negative velocities at  $\phi_{98} \sim 0.4$  may indicate overflowing material. The sine curve represents a fit to the H $\alpha$  radial velocities.

Table 1. Data Obtained for EX Hya during the 2000 May – June Observational Campaign.

Instrument	Observations <sup>a</sup>	Bandpass
Chandra	60 ks spectroscopy	1 – 20 Å
RXTE*	15 ks photometry and spectroscopy, 2000 May 18, 30	1 – 5 Å
USA	41.2 ks photometry	1 – 10 Å
EUVE	1000 ks photometry and spectroscopy	70 – 180 Å
FUSE	28 ks spectroscopy	800 – 1200 Å
HST	6 orbits spectroscopy	1100 – 1700 Å
APO*	2 nights spectroscopy, 2000 May 15 & 28	4200 – 5000, 6300 – 7300 Å
BO*	16 nights photometry, 2000 May 1–5, 7, 9, 10, 12–14, 25, 26 & Jun 2, 3, 7	$B, V, R$
RHO*	10 nights photometry, 2000 May 5, 8, 12, 18–20, 26–28, 31	$I$
UKIRT	1 night spectroscopy	1.9 – 2.5 $\mu\text{m}$

<sup>a</sup>Times given are in UT.

\*Data presented in this paper.

Table 2. Photometric frequencies appearing in the X-ray and optical photometry.

Observed frequency	Frequency (day <sup>-1</sup> )	Period (min)
$\omega$	21.48	67.03
$\omega/2$	10.74	134.05
$\Omega$	14.66	98.26
$\Omega/2$	7.33	196.51
$\omega - \Omega$	6.83	210.88
$\omega - 2\Omega$	7.83	183.98

Table 3.  $\Theta$  values of frequencies seen in the optical and X-ray thetagrams.

Frequency	$\Theta^a$		
	$B$	$I$	X-ray
$\omega$	0.42	0.56	0.76
$\Omega$	0.92	0.80	0.89
$\omega - \Omega$	0.55	0.64	...
$\omega - 2\Omega$	0.59	0.62	...

<sup>a</sup>95% confidence level is at  $\Theta = 0.97$  ( $B$ ),  $> 0.99$  ( $I$ ), 0.96 (X-ray), 99% confidence level is at  $\Theta = 0.95$  ( $B$ ),  $> 0.99$  ( $I$ ), 0.93 (X-ray)

Table 4. Sinusoidal fits to the spin phased photometry.

Bandpass	$A^a$	$B^a$	$\phi_0$
$B$	$-0.75 \pm 0.01$	$-0.20 \pm 0.01$	$0.87 \pm 0.02$
$V$	$-0.27 \pm 0.01$	$-0.17 \pm 0.01$	$0.87 \pm 0.02$
$R$	$-0.13 \pm 0.01$	$-0.17 \pm 0.01$	$0.87 \pm 0.02$
$I$	$0.02 \pm 0.01$	$0.13 \pm 0.01$	$0.82 \pm 0.02$
X-ray	$10.29 \pm 0.01$	$1.09 \pm 0.15$	$0.74 \pm 0.02$

<sup>a</sup> $A$  and  $B$  have units of  $\Delta m$  for  $BVRI$  and counts  $\text{sec}^{-1} \text{PCU}^{-1}$  for X-ray.